

Blood–spinal cord barrier disruption contributes to early motor-neuron degeneration in ALS-model mice

Ethan A. Winkler^{a,b,1}, Jesse D. Sengillo^{a,1}, Abhay P. Sagare^{a,1}, Zhen Zhao^a, Qingyi Ma^a, Edward Zuniga^a, Yaoming Wang^a, Zhihui Zhong^c, John S. Sullivan^a, John H. Griffin^d, Don W. Cleveland^{e,2}, and Berislav V. Zlokovic^{a,2}

^aZilkha Neurogenetic Institute, Center for Neurodegeneration and Regeneration, Department of Physiology and Biophysics, University of Southern California, Los Angeles, CA 90089; ^bSchool of Medicine and Dentistry, University of Rochester Medical Center, Rochester, NY 14642; ^cNational Chengdu Center for Safety Evaluation of Drugs, State Key Laboratory of Biotherapy, West China Hospital, Sichuan University, Chengdu, Sichuan, China; ^dDepartment of Molecular and Experimental Medicine, The Scripps Research Institute, La Jolla, CA 92037; and ^eLudwig Institute for Cancer Research, Department of Cellular and Molecular Medicine, and Department of Neuroscience, University of California, San Diego, La Jolla, CA 92093

Contributed by Don W. Cleveland, January 27, 2014 (sent for review December 27, 2013)

Humans with ALS and transgenic rodents expressing ALS-associated superoxide dismutase (*SOD1*) mutations develop spontaneous blood–spinal cord barrier (BSCB) breakdown, causing microvascular spinal-cord lesions. The role of BSCB breakdown in ALS disease pathogenesis in humans and mice remains, however, unclear, although chronic blood–brain barrier opening has been shown to facilitate accumulation of toxic blood-derived products in the central nervous system, resulting in secondary neurodegenerative changes. By repairing the BSCB and/or removing the BSCB-derived injurious stimuli, we now identify that accumulation of blood-derived neurotoxic hemoglobin and iron in the spinal cord leads to early motor-neuron degeneration in *SOD1*^{G93A} mice at least in part through iron-dependent oxidant stress. Using spontaneous or warfarin-accelerated microvascular lesions, motor-neuron dysfunction and injury were found to be proportional to the degree of BSCB disruption at early disease stages in *SOD1*^{G93A} mice. Early treatment with an activated protein C analog restored BSCB integrity that developed from spontaneous or warfarin-accelerated microvascular lesions in *SOD1*^{G93A} mice and eliminated neurotoxic hemoglobin and iron deposits. Restoration of BSCB integrity delayed onset of motor-neuron impairment and degeneration. Early chelation of blood-derived iron and antioxidant treatment mitigated early motor-neuronal injury. Our data suggest that BSCB breakdown contributes to early motor-neuron degeneration in ALS mice and that restoring BSCB integrity during an early disease phase retards the disease process.

amyotrophic lateral sclerosis | neurodegeneration

The blood–brain barrier (BBB) and blood–spinal cord barrier (BSCB) prevent entry of toxic circulating molecules and cells into the central nervous system (CNS) (1). Amyotrophic lateral sclerosis (ALS) is the most prominent adult motor-neuron disorder resulting in progressive motor-neuron loss in the spinal cord, brainstem, and motor cortex (2). Most ALS cases are sporadic (90%) whereas 10% are familial ALS. Over twenty independent studies in postmortem human tissue and cerebrospinal fluid (CSF) sampling from living ALS patients have established that the BBB and BSCB are damaged in familial and sporadic ALS, as reviewed elsewhere (1, 3). This BBB and BSCB disruption has been shown by spinal-cord and/or motor-cortex accumulation of different plasma proteins (e.g., IgG, fibrin, thrombin), erythrocytes, erythrocyte-derived hemoglobin and iron-containing hemosiderin, elevated CSF/serum albumin ratios, and diminished expression or degradation of the BSCB tight-junction proteins (1, 3–5). Deposition of hemoglobin-derived iron within the CNS has also been shown in ALS patients (3, 6, 7). Because human postmortem studies reflect, however, end-stage disease, it has remained unclear as to which stage of disease is enhanced by BSCB disruption. Longitudinal CSF or BSCB imaging studies have yet to be performed in living ALS patients (3) to clarify whether spinal-cord vascular dysfunction contributes to early- or late-stage disease.

Transgenic rodents expressing human ALS-associated Cu/Zn superoxide dismutase (*SOD1*) mutations that represent 20% of all familial cases also develop a spontaneous BBB/BSCB disruption (8–12) similar to vascular pathology reported in humans (1, 3–7). Mice with a chronic BBB disruption due to aberrant signal transduction between the central nervous system endothelial cells and pericytes or astrocytes and pericytes develop a chronic BBB opening accompanied by accumulation of toxic blood-derived products in the central nervous system and secondary functional and structural neuronal changes (13–15).

To determine whether BSCB disruption contributes to fatal paralytic disease caused by expression of an ALS-causing mutant, we now report how perturbing the BSCB, repairing the BSCB, and/or removing the BSCB-derived injurious stimuli influence development of disease in *SOD1*^{G93A} mice that develop a spontaneous BSCB breakdown (8, 9, 12).

Results and Discussion

Microvascular Lesions Contribute to Early Motor-Neuron Impairment and Degeneration. To further perturb the BSCB in *SOD1*^{G93A} mice, we used a low dose of warfarin, an anticoagulant (16). Although treatment with a high dose of warfarin produces massive

Significance

The blood–spinal cord barrier (BSCB) is damaged in human ALS and rodents expressing ALS-associated superoxide dismutase mutations. The role of BSCB breakdown in disease pathogenesis remains, however, unclear. Early motor-neuron dysfunction and injury are now shown to be proportional to the degree of BSCB disruption, and early protection of the BSCB integrity with an activated protein C analog is found to delay onset of motor-neuron impairment and degeneration. Altogether, these findings in mice show that BSCB breakdown plays a role in early-stage disease pathogenesis and that restoring BSCB integrity retards the disease process. These findings are relevant to the corresponding disease mechanism in human ALS in which ALS-associated vascular pathology is associated.

Author contributions: E.A.W., J.H.G., D.W.C., and B.V.Z. designed research; E.A.W., J.D.S., A.P.S., Z. Zhao, Q.M., E.Z., Y.W., Z. Zhong, and J.S.S. performed research; J.H.G. and D.W.C. contributed new reagents/analytic tools; E.A.W., J.D.S., A.P.S., Z. Zhao, Q.M., E.Z., Y.W., Z. Zhong, J.S.S., and B.V.Z. analyzed data; and E.A.W., D.W.C., and B.V.Z. wrote the paper.

Conflict of interest statement: B.V.Z. is the scientific founder of ZZ Biotech, a start-up biotechnology company that is developing an activated protein C analog for stroke with possible implications in other neurological disorders. J.H.G. is a member of the Scientific Advisory Board of ZZ Biotech.

Freely available online through the PNAS open access option.

¹E.A.W., J.D.S., and A.P.S. contributed equally to this work.

²To whom correspondence may be addressed. E-mail: zlokovic@usc.edu or dcleveland@ucsd.edu.

This article contains supporting information online at www.pnas.org/lookup/suppl/doi:10.1073/pnas.1401595111/-DCSupplemental.

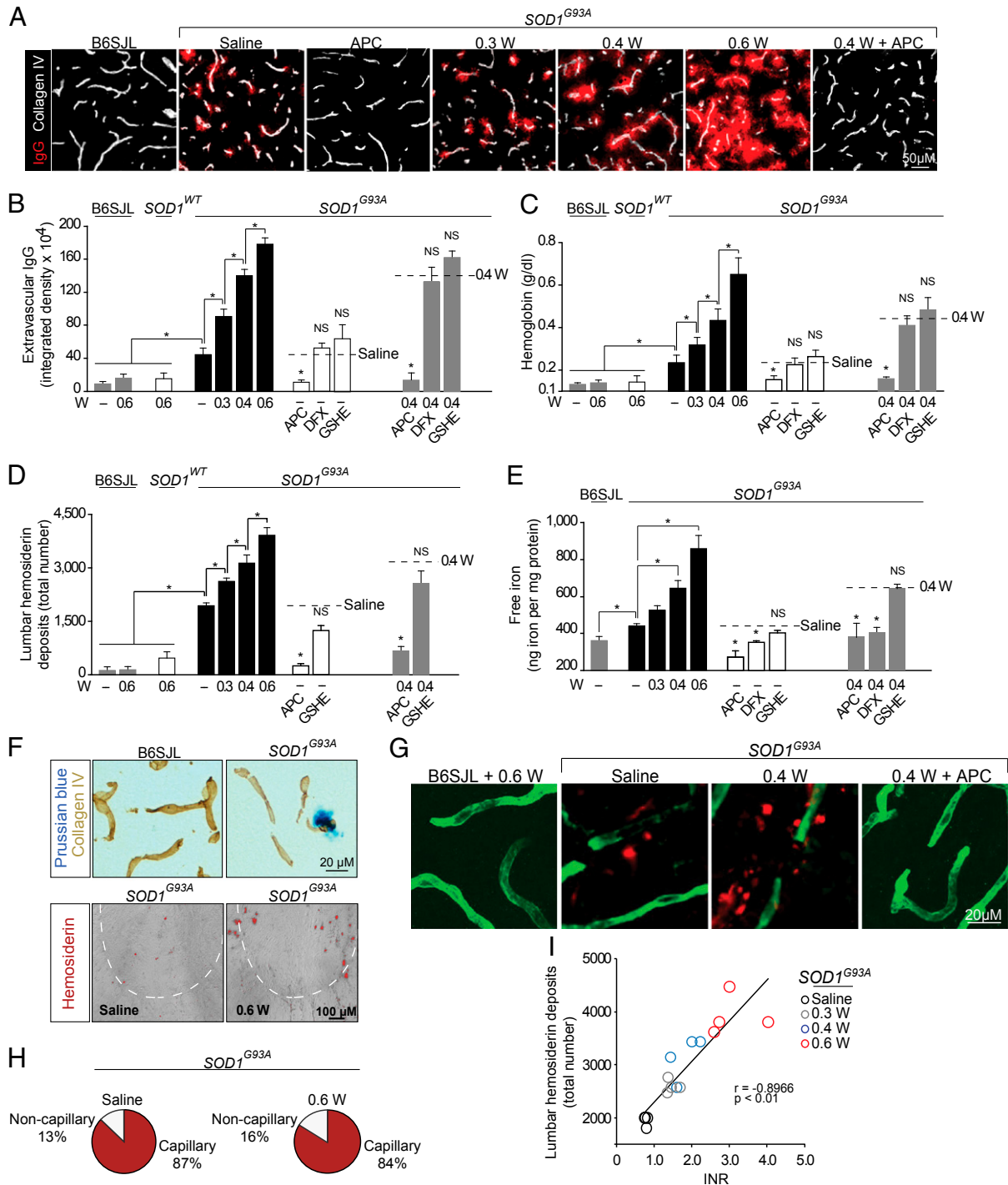


Fig. 1. Early microvascular lesions in *SOD1^{G93A}* mice: acceleration by Warfarin and protection by 5A-APC. (A–E) IgG (A and B), hemoglobin (C), hemosiderin (D), and free iron (E) in the lumbar anterior horn of *SOD1^{G93A}* mice receiving from 35 to 95 d saline, 0.3–0.6 mg·kg⁻¹·d⁻¹ warfarin (W), and/or 100 μ g·kg⁻¹·d⁻¹ 5A-APC (APC), 100 mg·kg⁻¹·d⁻¹ deferoxamine mesylate (DFX), or 50 mg·kg⁻¹·d⁻¹ glutathione monoethyl ester (GSHE) with either saline or warfarin (0.4 mg·kg⁻¹·d⁻¹). B6SJL littermates and *SOD1^{WT}* mice received saline or warfarin (0.6 mg·kg⁻¹·d⁻¹). (F, Upper) Prussian blue-positive hemosiderin deposits (blue) and collagen IV-positive capillaries (brown) in lumbar cord anterior horn of 95-d-old B6SJL littermate and saline-treated *SOD1^{G93A}* mouse. (Lower) Perl's-positive hemosiderin deposits (red) in 95-d-old *SOD1^{G93A}* mouse receiving saline or 0.6 mg·kg⁻¹·d⁻¹ warfarin. Broken line denotes boundary of the anterior horn. (G) Collagen IV-positive capillaries (green) and CD235a-positive erythrocytes (red) in the lumbar anterior horn of 95-d-old B6SJL littermate receiving 0.6 mg·kg⁻¹·d⁻¹ warfarin and *SOD1^{G93A}* mice receiving saline, 0.4 mg·kg⁻¹·d⁻¹ warfarin or 0.4 mg·kg⁻¹·d⁻¹ warfarin and 5A-APC (100 μ g·kg⁻¹·d⁻¹). (H) Percentage of capillary-associated and noncapillary hemosiderin deposits in 95-d-old *SOD1^{G93A}* mice receiving saline or warfarin (0.6 mg·kg⁻¹·d⁻¹); $n = 4$ –5 mice per group. (I) Positive correlation between the number of lumbar hemosiderin deposits and the degree of anticoagulation determined as international normalized ratio (INR) in 95-d-old *SOD1^{G93A}* mice receiving saline or warfarin (0.3–0.6 mg·kg⁻¹·d⁻¹). Individual data points from four to five animals per group; r , Pearson's correlation. In B–E, mean \pm SEM, $n = 3$ –5 mice per group. * $P < 0.05$; NS, nonsignificant. In B–E, APC, DFX, and GSHE treatments were compared with the respective saline or warfarin treatments as indicated by broken lines.

cerebral hemorrhage and lethality in rodent models as the result of hemorrhagic stroke and brain injury (17–19), low-dose warfarin (0.3, 0.4, and 0.6 mg/kg daily) from day 35–95 postnatal provided a stable, chronic low level of anticoagulation activity in *SOD1^{G93A}* mice accompanied by an increase of the mean international normalized ratio (INR) values of 1.3, 2.0, and 2.9, respectively (Fig. S1 *A* and *B*). Low-dose warfarin did not alter hematocrit, indicating no systemic bleeding (Fig. S1 *C*). Anticoagulated *SOD1^{G93A}* mice, but not anticoagulated nontransgenic littermates or *SOD1^{WT}* mice with an intact BSCB (9), developed an increased number of microvascular lesions compared with saline-treated *SOD1^{G93A}* mice, as indicated by dose-dependent spinal-cord accumulation of blood-derived IgG, hemoglobin, hemosiderin, free iron, and erythrocytes (Fig. 1 *A–G*). Most (~85%) of microvascular lesions determined by hemosiderin deposits (20–50 μm in diameter) were associated with spinal-cord capillaries ($\leq 6 \mu\text{m}$ in diameter) compared with noncapillary microvessels (6–40 μm in diameter) both in saline-treated and warfarin-treated *SOD1^{G93A}* mice (Fig. 1 *H*). A positive correlation between the number of hemosiderin deposits and INR values in individual *SOD1^{G93A}* mice (Fig. 1 *I*) indicated that the microvascular damage is proportional to the degree of warfarin anticoagulation.

Warfarin was not toxic to cultured CNS endothelial cells (Fig. S2 *A–C*) and did not alter endothelial expression of tight-junction proteins—including zonula occludens (ZO1), occludin, and claudin-5 (Fig. S2 *D* and *E*) and/or uptake of different-size dextran tracers (Fig. S2 *F*). In vivo, warfarin did not affect spinal-cord capillary density (Fig. S2 *G* and *H*) and/or BSCB integrity (Fig. 1 *B–E*) in nontransgenic littermates or *SOD1^{WT}* mice and did not alter the expression of multiple transporters in spinal-cord capillaries of *SOD1^{G93A}* mice (Table S1). Thus, increased microvascular lesions induced by warfarin treatment in *SOD1^{G93A}* mice arise from its anticoagulant activity, not via direct actions on endothelium.

Microvascular lesions in *SOD1^{G93A}* mice contain blood-derived hemoglobin that releases free iron, which can catalyze formation of neurotoxic free radical species, as previously shown in in vitro models of motor-neuronal cell injury (20) and more recently in N2a-SOD1^{G85R} neural cell injury (11). Consistent with spinal-cord accumulation of neurotoxic blood-derived products (Fig. 1 *A–G*), *SOD1^{G93A}* mice treated with warfarin (0.3, 0.4, and 0.6 mg/kg daily) beginning ~70 d before our measure of typical disease onset developed a dose-dependent acceleration in disease onset [determined by rotarod by 11, 18, and 26 d compared with saline-treated *SOD1^{G93A}* mice, respectively (Fig. 2 *A* and *B*)]. In individual *SOD1^{G93A}* mice, onset of motor impairment was directly proportional to the number of perivascular hemosiderin deposits (Fig. 2 *C*). Correspondingly, presymptomatic warfarin treatment shortened lifespan of *SOD1^{G93A}* mice (Fig. S3 *A* and *B*) in a dose-dependent manner. Disease duration (Fig. S3 *C*) was not significantly affected, consistent with previous studies that have demonstrated disease progression to be driven by mutant SOD1 synthesis within inflammatory microglia and astrocytes (21–26). Although, mutant SOD1 transgenic rats develop BBB and BSCB breakdown (10), the contribution of BBB damage to neurological disease in SOD1 transgenic rodents is presently unknown, as well as whether *SOD1^{G93A}* mice develop or not a generalized or regional BBB breakdown (in the motor cortex) that might contribute to the observed accelerated disease phenotype.

Compared with saline-treated *SOD1^{G93A}* mice, warfarin-treated *SOD1^{G93A}* mice showed dose-dependent loss of choline acetyltransferase (ChAT)-positive motor neurons (27) (Fig. 3 *A* and *B*), loss of neuritic density (Fig. 3 *C* and *D*), and an increase in ubiquitin-positive aggregates (28) (Fig. 3 *E* and *F*). In individual *SOD1^{G93A}* mice with spontaneous or accelerated vascular lesions, markers of motor-neuronal degeneration strongly

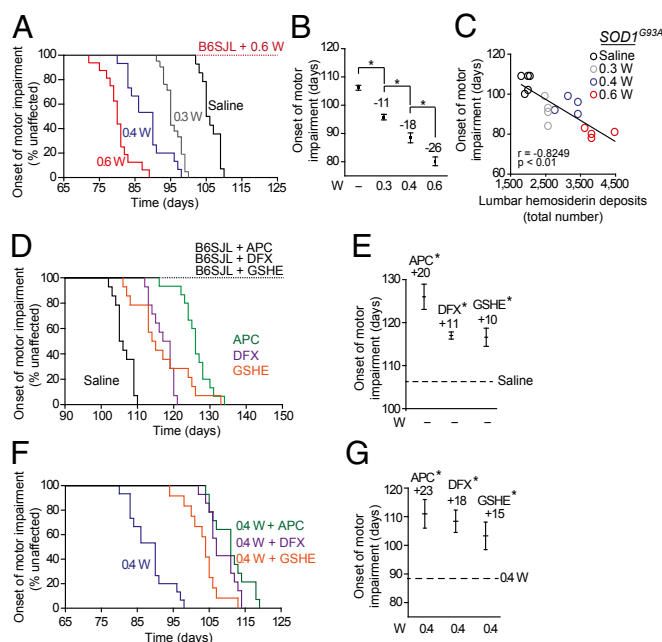


Fig. 2. Onset of motor impairment and prevention in *SOD1^{G93A}* mice with spontaneous and accelerated microvascular lesions. (*A* and *B*) Cumulative probability (*A*) and mean age (*B*) of motor impairment in *SOD1^{G93A}* mice treated with saline ($n = 14$) or 0.3 ($n = 21$), 0.4 ($n = 15$), and 0.6 ($n = 16$) $\text{mg}\cdot\text{kg}^{-1}\cdot\text{d}^{-1}$ warfarin (W) from day 35 postnatal. Acceleration of motor symptoms in days relative to saline is provided above each group. Values in *B*, mean \pm SEM, * $P < 0.05$. Nontransgenic B6SJL littermates ($n = 14$) received 0.6 $\text{mg}\cdot\text{kg}^{-1}\cdot\text{d}^{-1}$ warfarin. (*C*) Negative correlation between onset of motor impairment and number of lumbar hemosiderin deposits in *SOD1^{G93A}* mice treated with saline or warfarin (0.3–0.6 $\text{mg}\cdot\text{kg}^{-1}\cdot\text{d}^{-1}$). Individual data points are from four to five mice per group; r , Pearson's correlation. (*D* and *E*) Cumulative probability (*D*) and mean age (*E*) of motor impairment in *SOD1^{G93A}* mice treated daily with saline ($n = 14$), 100 $\mu\text{g}/\text{kg}$ 5A-APC ($n = 15$), 100 mg/kg DFX ($n = 14$), or 50 mg/kg GSHE ($n = 14$) from day 35 postnatal. Delay of motor symptoms in days relative to saline is provided above each group. Values in *E*, mean \pm SEM, * $P < 0.05$ compared with saline. Nontransgenic B6SJL littermates ($n = 14$ per group) received APC, DFX, or GSHE. (*F* and *G*) Cumulative probability (*F*) and mean age (*G*) of motor impairment in *SOD1^{G93A}* mice treated with 0.4 $\text{mg}\cdot\text{kg}^{-1}\cdot\text{d}^{-1}$ warfarin ($n = 15$) and 100 $\mu\text{g}\cdot\text{kg}^{-1}\cdot\text{d}^{-1}$ 5A-APC ($n = 14$), 100 $\text{mg}\cdot\text{kg}^{-1}\cdot\text{d}^{-1}$ DFX ($n = 14$), or 50 $\text{mg}\cdot\text{kg}^{-1}\cdot\text{d}^{-1}$ GSHE ($n = 14$) from day 35 postnatal. Delay of motor symptoms in days relative to 0.4 mg/kg warfarin is provided above each group. Values in *G*, mean \pm SEM, * $P < 0.05$ compared with 0.4 $\text{mg}\cdot\text{kg}^{-1}\cdot\text{d}^{-1}$ warfarin.

correlated with the magnitude of vascular damage determined by the number of hemosiderin deposits (Fig. 3 *D* and *G*).

Warfarin did not exert direct neuronal toxic effects. For example, warfarin did not affect motor function in nontransgenic controls with an intact BSCB (Fig. 2 *A*), was not toxic to primary cultured neurons from *SOD1^{G93A}* mice (Fig. S4 *A–C*), did not cause neuronal degeneration in vivo in nontransgenic littermates with an intact BSCB (Fig. 3 *D–F*), and did not interfere with the vitamin K-dependent synthetic pathway (29) as shown by normal levels of sphingolipids or Gas6 in spinal cord (Fig. S4 *G* and *H*). Warfarin treatment was also not associated with pro-inflammatory responses (Fig. S5). Blood glucose, liver, and renal function tests showed no difference in *SOD1^{G93A}* mice treated with saline compared with warfarin (Fig. S6 *A–F*), suggesting that warfarin did not lead to generalized tissue dysfunction.

SOD1^{G93A} mice with spontaneous and/or accelerated vascular damage showed increased oxidant stress (Fig. 4 *A*) that correlated with increased levels of free iron in the spinal cord (Fig. 4 *B*), increased oxidation of human SOD1, and the appearance of higher molecular weight insoluble toxic SOD1 oxidized species

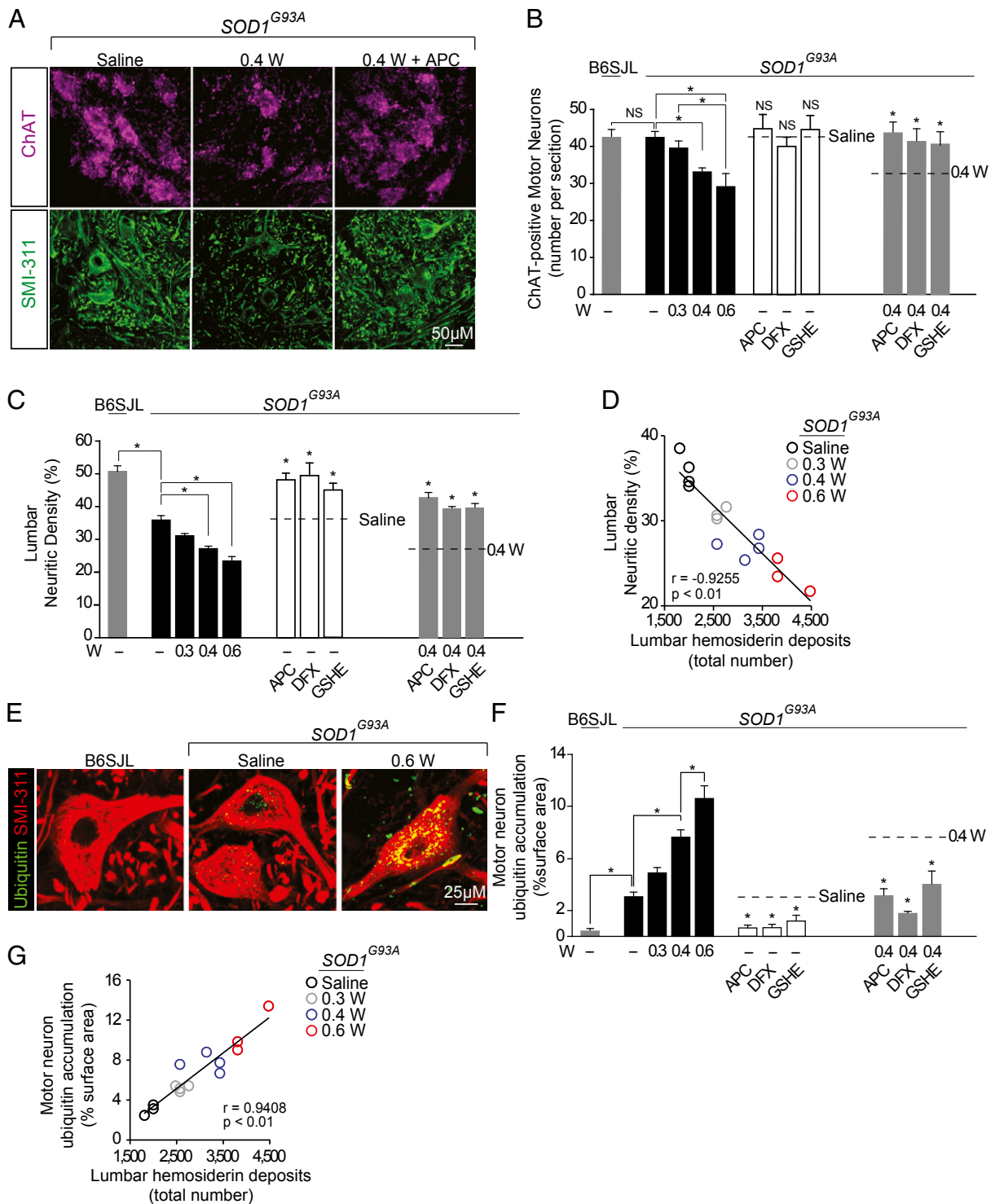


Fig. 3. Early motor-neuron degenerative changes and prevention in *SOD1^{G93A}* mice with spontaneous and accelerated microvascular lesions. (A–C) ChAT-positive motor neurons (magenta) and SMI-311-positive neurites (green) (A) and quantification of motor neurons (B) and neuritic density (C) in lumbar spinal cord of 95-d-old nontransgenic littermates and *SOD1^{G93A}* mice treated with saline, 0.3–0.6 mg·kg⁻¹·d⁻¹ warfarin (W), or 100 μ g·kg⁻¹·d⁻¹ 5A-APC, 100 mg·kg⁻¹·d⁻¹ DFX, or 50 mg·kg⁻¹·d⁻¹ GSHE with saline or 0.4 mg·kg⁻¹·d⁻¹ warfarin. (D) Negative correlation between SMI-311-positive neurites and lumbar hemisiderin deposits of 95-d-old individual *SOD1^{G93A}* mice treated with saline or 0.3–0.6 mg·kg⁻¹·d⁻¹ warfarin. r , Pearson's correlation; $n = 4$ –5 animals per group. (E) Ubiquitin-positive accumulates (green) in motor neurons (red, visualized with SMI-311) in the lumbar anterior horn in 95-d-old *SOD1^{G93A}* mice treated with saline or 0.6 mg·kg⁻¹·d⁻¹ warfarin. B6SJL, a nontransgenic littermate control. (F) Quantification of ubiquitin accumulation in motor neurons in mice from B. (G) Positive correlation between motor-neuron ubiquitin accumulation and the number of lumbar hemisiderin deposits in *SOD1^{G93A}* mice treated with saline or 0.3–0.6 mg·kg⁻¹·d⁻¹ warfarin. Each point is an individual data point; r , Pearson's correlation; $n = 3$ –5 mice per group. In B, C, and F, values are mean \pm SEM; $n = 3$ –5 mice per group. * $P < 0.05$; NS, nonsignificant. In B, C, and F, APC, DFX, and GSHE treatments were compared with the respective saline and warfarin treatments as indicated by broken lines.

(Fig. 4 C–E). SOD1 oxidation can promote its misfolding, aggregation, and toxicity, which—according to some studies—may be common to sporadic ALS and familial ALS caused by *SOD1* mutations (30–34). Double staining for ChAT and 3-nitrotyrosine, an oxidative stress cellular marker, confirmed early motor-neuron oxidant stress in *SOD1*^{G93A} mice with a spontaneous BSCB breakdown and a further, dose-dependent increase in the number of motor neurons under oxidant stress in *SOD1*^{G93A} mice with warfarin-accelerated vascular damage (Fig. 4 F and G).

BSCB Repair Delays Onset of Motor-Neuron Impairment and Degeneration. To determine whether BSCB repair can delay onset of motor-neuron injury in *SOD1*^{G93A} mice, we used an activated protein C (APC) mutant, 5A-APC, that retains cell-signaling properties but lacks >90% of the anticoagulant activity (35). 5A-APC protects the integrity of CNS endothelial barriers in different models of acute and chronic CNS injury (36). APC cell signaling activates Rac1-dependent stabilization of the cytoskeleton, thereby enhancing the endothelial barrier integrity (37). 5A-APC treatment (100 μg/kg daily) beginning early at postnatal day 35 completely normalized the BSCB integrity in *SOD1*^{G93A} mice with either spontaneous or warfarin-accelerated microvascular lesions as indicated by elimination of IgG, hemoglobin, hemosiderin, and free iron deposits (Fig. 1 A–E). Maintenance of BSCB integrity significantly delayed onset of motor impairment [by 20 and 23 d compared with saline (Fig. 2 E and F) and warfarin treatment (Fig. 2 G and H), respectively] in *SOD1*^{G93A} mice with both spontaneous and accelerated microvascular lesions. 5A-APC prevented early motor-neuron degenerative changes in *SOD1*^{G93A} mice involving spontaneous and accelerated BSCB breakdown, as shown by normalization of neuritic density and elimination of ubiquitin-positive deposits from motor neurons (Fig. 3 C and F), and normalized the reduced number of ChAT-positive motor neurons in warfarin-treated *SOD1*^{G93A} mice (Fig. 3B). Its beneficial effects were associated with early reduction in oxidant stress as shown by reduced levels of oxidized protein carbonyls in the spinal cord (Fig. 4A), reduction in SOD1 oxidative damage as shown by diminished levels of higher molecular weight insoluble toxic SOD1 oxidized species (Fig. 4C), and reduced oxidant motor-neuron injury as shown by diminished number of ChAT-positive motor neurons that were positive for 3-nitrotyrosine, an oxidative stress cellular marker (Fig. 4 F and G).

At presymptomatic ages, *SOD1*^{G93A} mice develop diminished levels of spinal-cord capillary tight junction proteins including ZO1, occluding, and claudin-5 (9) (Fig. S7 A–C), which provides a molecular basis for early BSCB breakdown. 5A-APC treatment beginning at postnatal day 35 normalized spinal-cord capillary levels of ZO-1, occluding, and claudin-5 in *SOD1*^{G93A} mice with either spontaneous or warfarin-accelerated lesions (Fig. S7 A–C), consistent with its effect on preventing early BSCB breakdown (Fig. 1 A–E and G). Warfarin treatment did not affect tight junction protein expression (Fig. S7 A–C). In saline-treated and warfarin-treated *SOD1*^{G93A} mice, a presymptomatic increase in hemosiderin deposits (Fig. S7D) did not result in a detectable increase in microglial and astrocytic responses (Fig. S7 E–G), confirming that early BSCB disruption precedes a detectable inflammatory response in *SOD1*^{G93A} mice (9).

In our prior work, we reported that APC treatment beginning 1 wk after motor-neuron impairment influenced multiple components of late-stage disease in *SOD1*^{G93A} mice, including suppression of *SOD1* in motor neurons and microglia by ~40–50% (11). In contrast, early 5A-APC treatment had no effect on mutant SOD1 protein or mRNA expression in spinal cord and/or motor neurons of *SOD1*^{G93A} mice, as revealed by analysis of spinal-cord lysates from 5A-APC-treated *SOD1*^{G93A} mice with spontaneous or warfarin-accelerated microvascular lesions (Fig. S7 H

and I) and enriched motor-neuron cell populations from 5A-APC and warfarin-treated *SOD1*^{G93A} mice (Fig. S7 J and K). Thus, *SOD1* down-regulation in motor neurons cannot be the primary contributor to APC's therapeutic effects seen during early disease. Rather, the effects of APC on gene expression profiles of different cell types under stress show a remarkable complexity in the diverse effects mediated by APC (37). Importantly, BSCB protection is the sole beneficial effect of APC treatment seen during early disease stage in *SOD1*^{G93A} mice.

When 5A-APC was given before early disease (and before a detectable microglia response), the strong anti-inflammatory effect previously reported for 5A-APC therapy, including inhibition of *SOD1* expression in microglia (11), was not found. A continuation of early presymptomatic 5A-APC treatment from day 35 postnatal until clinical death significantly increased lifespan [by 40 d (29%) and 42 d (35%) compared with saline (Fig. S8 A and B) and warfarin treatment (Fig. S9 A and B), respectively] and extended disease progression phase [by 20 d (79%) and 23 d (88%) compared with saline (Fig. S8C) and warfarin treatment (Fig. S9C), respectively] in *SOD1*^{G93A} mice with both spontaneous and accelerated microvascular lesions. These data demonstrate that early presymptomatic treatment with 5A-APC of *SOD1*^{G93A} mice with either spontaneous or warfarin-accelerated microvascular lesions has greater beneficial effects on lifespan than the previously reported 28 d (25%) extension of lifespan obtained with postsymptomatic treatment of *SOD1*^{G93A} mice with 5A-APC beginning 1 wk after phenotypic disease onset (determined by weight loss) (11). Greater overall beneficial effects of an early treatment of *SOD1*^{G93A} mice with 5A-APC compared with late postsymptomatic treatment (11) are likely attributable to repair and/or maintenance of BSCB integrity, thereby preventing entry and accumulation of neurotoxic blood-derived products within the spinal cord during an initial disease phase (Fig. 1 A–G).

Iron Chelation Mitigates Early Motor-Neuron Injury. Iron chelation has been reported to protect cultured motor neurons from hemoglobin-induced injury (26) and to extend lifespan (without changes in blood vessels and/or BSCB integrity to blood-derived iron) when applied at a relatively late disease stage in *SOD1*^{G37R} mice that have already induced higher levels of expression of iron homeostasis proteins in neurons and astrocytes (38). To determine whether eliminating the BSCB-derived injurious stimuli can similarly delay early onset of motor-neuronal injury, we used treatment with deferoxamine (DFX) beginning at an early point postnatally (day 35) to chelate blood-derived iron in *SOD1*^{G93A} mice that develop spontaneous and warfarin-accelerated vascular lesions. DFX treatment did not alter BSCB permeability to IgG, hemoglobin, or hemosiderin in *SOD1*^{G93A} mice (Fig. 1 B–D), but significantly reduced early free iron accumulation (Fig. 1E and Fig. S10A), accompanied by delayed onset [by 11 and 18 d compared with saline (Fig. 2 E and F) and warfarin treatment (Fig. 2 G and H), respectively] of motor impairment in *SOD1*^{G93A} mice with spontaneous and accelerated microvascular lesions. DFX delayed early motor-neuron degenerative changes (Fig. 3 C and F) and loss of ChAT-positive motor neurons in warfarin-treated *SOD1*^{G93A} mice (Fig. 3B), and reduced oxidant stress, SOD1 oxidative changes, and oxidant motor-neuron injury (Fig. 4 A, D, and G). Early motor-neuron dysfunction in the *SOD1*^{G93A} mice occurred in the absence of changes in the expression of iron homeostasis proteins in the spinal cord (including the divalent-metal transporter 1, transferrin-receptor 1, iron exporter ferroportin, two ferroxidases, and ferritin heavy and light chains) (Fig. S10B). Iron chelation also extended lifespan [by 13 d (10%) and 20 d (18%) compared with saline (Fig. S8 A and B) and warfarin treatment (Fig. S9 A and B), respectively] but did not affect significantly disease progression compared with saline (Fig. S8C) and warfarin treatment

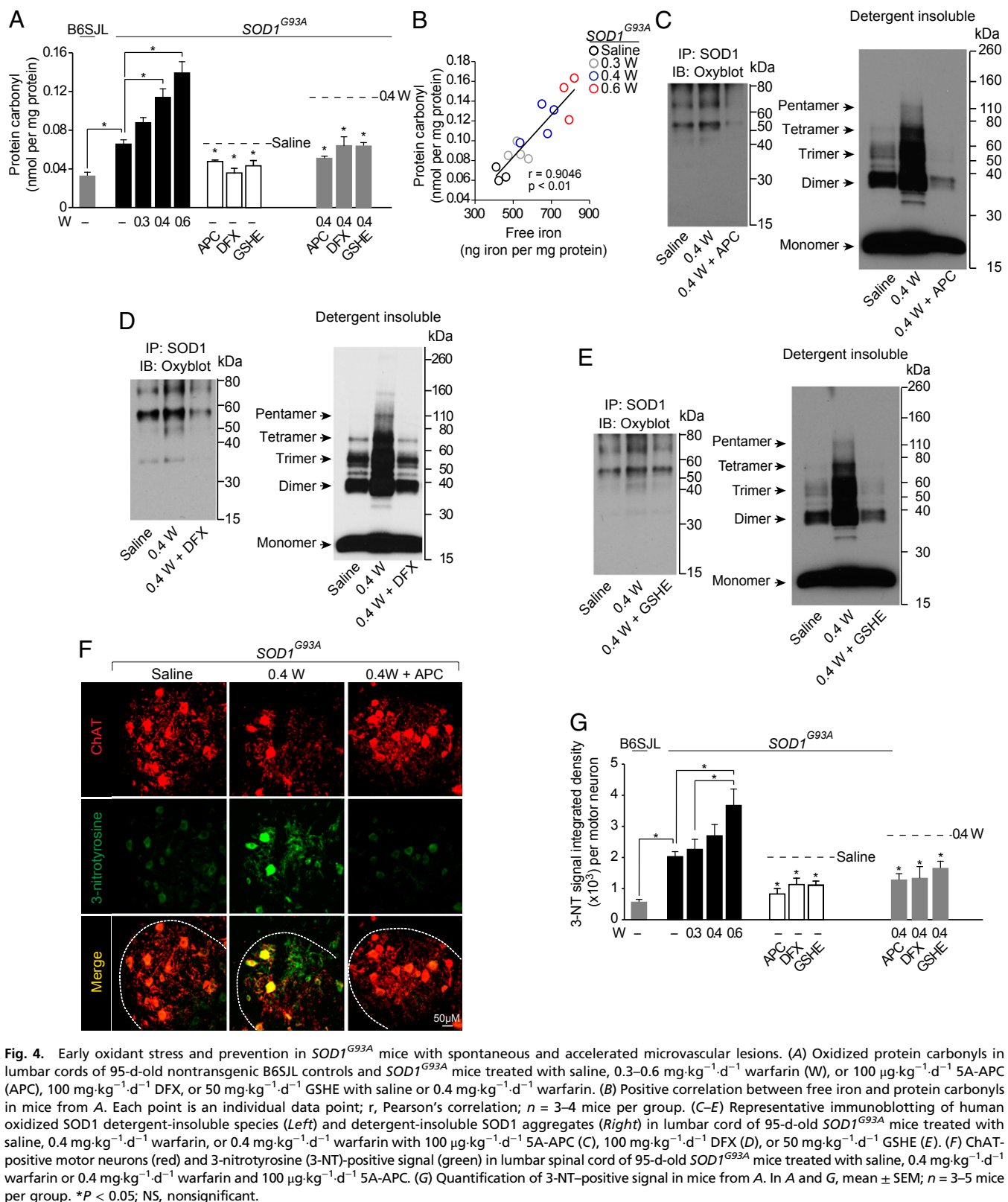


Fig. 4. Early oxidant stress and prevention in $SOD1^{G93A}$ mice with spontaneous and accelerated microvascular lesions. (A) Oxidized protein carbonyls in lumbar cords of 95-d-old nontransgenic B6SJL controls and $SOD1^{G93A}$ mice treated with saline, 0.3–0.6 mg·kg⁻¹·d⁻¹ warfarin (W), or 100 μ g·kg⁻¹·d⁻¹ 5A-APC (APC), 100 mg·kg⁻¹·d⁻¹ DFX, or 50 mg·kg⁻¹·d⁻¹ GSHE with saline or 0.4 mg·kg⁻¹·d⁻¹ warfarin. (B) Positive correlation between free iron and protein carbonyls in mice from A. Each point is an individual data point; *r*, Pearson's correlation; *n* = 3–4 mice per group. (C–E) Representative immunoblotting of human oxidized SOD1 detergent-insoluble species (Left) and detergent-insoluble SOD1 aggregates (Right) in lumbar cord of 95-d-old $SOD1^{G93A}$ mice treated with saline, 0.4 mg·kg⁻¹·d⁻¹ warfarin, or 0.4 mg·kg⁻¹·d⁻¹ warfarin with 100 μ g·kg⁻¹·d⁻¹ 5A-APC (C), 100 mg·kg⁻¹·d⁻¹ DFX (D), or 50 mg·kg⁻¹·d⁻¹ GSHE (E). (F) ChAT-positive motor neurons (red) and 3-nitrotyrosine (3-NT)-positive signal (green) in lumbar spinal cord of 95-d-old $SOD1^{G93A}$ mice treated with saline, 0.4 mg·kg⁻¹·d⁻¹ warfarin or 0.4 mg·kg⁻¹·d⁻¹ warfarin and 100 μ g·kg⁻¹·d⁻¹ 5A-APC. (G) Quantification of 3-NT-positive signal in mice from A. In A and G, mean \pm SEM; *n* = 3–5 mice per group. **P* < 0.05; NS, nonsignificant.

(Fig. S9C), respectively, in $SOD1^{G93A}$ mice with both spontaneous and accelerated microvascular lesions.

These DFX iron chelator data offer strong support for a model in which an early presymptomatic accumulation of iron in the spinal cord of $SOD1^{G93A}$ mice with spontaneous and ac-

celerated microvascular lesions (Fig. 1E and Fig. S10A) reflects increased influx of blood-derived iron across a disrupted BSCB, as indicated by extravasation of blood's erythrocytes (Fig. 1G) resulting in deposition of iron-containing proteins hemoglobin and hemosiderin (Fig. 1C and D) and release of free iron (20).

Compared with APC therapy, the beneficial effects of DFX on lifespan were more modest, as would be anticipated by the inability of chelation to inhibit influx of other potentially neurotoxic blood-derived products that do not depend on iron neurotoxicity, including thrombin and fibrin (14, 15), each of which can freely diffuse across a disrupted BSCB. Moreover, iron chelation by DFX does not provide direct anti-inflammatory and direct motor-neuronal protective effects that have been shown to contribute to 5A-APC's beneficial effects during late disease stage (11).

Antioxidant Treatment Mitigates Early Motor-Neuron Injury. Finally, we tested whether glutathione monoethyl ester (GSHE), an antioxidant that in its reduced form has been shown to counteract oxidative damage in rodents with spinal-cord injury (39), could delay disease onset in *SOD1^{G93A}* mice. GSH is quantitatively the most important endogenous recycled antioxidant. Reduced GSH levels accelerate neurological deficits in *SOD1^{G93A}* mice (40). GSHE is cell-permeable and is transported across the BSCB (in contrast to GSH, which is poorly transported into cells). GSHE did not alter the BSCB integrity or iron accumulation in *SOD1^{G93A}* mice (Fig. 1 *B–E*), but onset of motor symptoms in mice with either spontaneous or accelerated microvascular lesions was delayed by 10 and 15 d, respectively, compared with saline (Fig. 2 *E* and *F*) or when administered along with warfarin (Fig. 2 *G* and *H*). GSHE also delayed early motor-neuron degenerative changes in *SOD1^{G93A}* mice with both spontaneous and accelerated microvascular lesions (Fig. 3 *C–F*) and prevented early loss of ChAT-positive motor neurons in warfarin-treated *SOD1^{G93A}* mice (Fig. 3*B*). As expected, GSHE reduced early oxidant stress (measured by oxidized protein carbonyl content), SOD1 oxidative changes, and early oxidant motor-neuron injury (Fig. 4 *A*, *E*, and *G*).

Presymptomatic GSHE treatment modestly increased lifespan [by 10 d (10%) and 14 d (13%) compared with saline (Fig. S8 *A* and *B*) and warfarin treatment (Fig. S9 *A* and *B*), respectively] but, similar to DFX, did not affect disease progression phase compared with either saline (Fig. S8*C*) or warfarin treatment (Fig. S9*C*), respectively, in *SOD1^{G93A}* mice with spontaneous and/or accelerated microvascular lesions. GSHE effects on lifespan were proportional to the magnitude of its beneficial effects on delaying disease onset compared with saline (Fig. 2 *D* and *E*) and warfarin (Fig. 2 *F* and *G*), respectively. Like iron chelation, the overall benefits of GSHE treatment were less pronounced than seen with 5A-APC, possibly related to a lack of significant GSHE effect on BSCB integrity, as well as lack of direct anti-inflammatory and neuroprotective effects on cells that have been shown to play an important role in 5A-APC effects on lifespan (11).

Conclusions and Future Directions. Studies in mice have demonstrated that direct SOD1 damage within motor neurons is a central component of driving disease initiation but not disease progression (21, 25, 41) whereas progression is predominantly determined by responses within microglia and astrocytes (21–26). Here, we have focused on events occurring in the early disease phase. Early oxidative damage has been repeatedly reported in mutant SOD1 mice, including mRNA oxidation (42). Our efforts now provide a molecular mechanism for such damage and link intraneuronal damage to initial disease. We have found that early BSCB breakdown (spontaneous and/or accelerated) directly contributes to early motor-neuron injury in *SOD1^{G93A}* mice and that restoring the BSCB integrity and/or eliminating the BSCB-derived sources of neuronal injury delay initial motor-neuron degeneration (Fig. 5). Our findings in ALS mice raise questions as to whether similar BSCB disruption in patients with familial and/or sporadic ALS contributes to early motor-neuron degeneration in humans. Future studies using models with a

Early Stage BSCB Breakdown

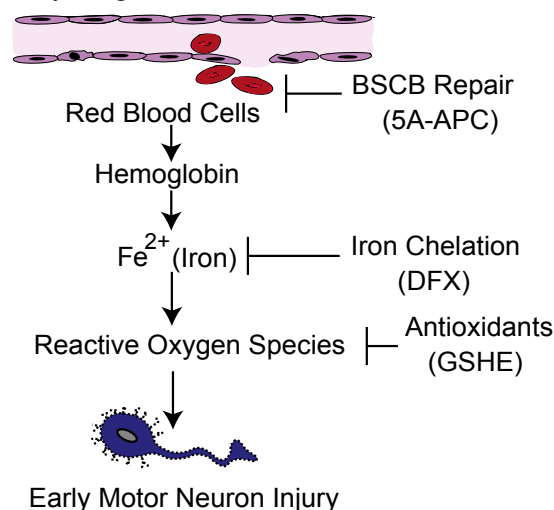


Fig. 5. A schematic illustrating how early blood–spinal cord barrier (BSCB) breakdown initiates motor-neuron injury and how BSCB-directed treatments blocking different steps in the BSCB pathogenic cascade can prevent early motor-neuron injury.

chronic BBB/BSCB disruption independent of human SOD1 transgene expression, such as pericyte-deficient mice (13, 14), are now needed to explore whether early motor-neuron degeneration can be initiated by BSCB disruption in the absence of SOD1 motor-neuronal damage.

Materials and Methods

Reagents. Warfarin sodium, DFX, and GSHE were obtained from Sigma-Aldrich. Recombinant mouse 5A-APC (RR230/231AA and KKK192-194AAA) variant was purified as described (37).

Animals. Male *SOD1^{G93A}* mice were purchased from The Jackson Laboratory. Mice were treated with daily i.p. injections of saline, warfarin sodium (0.3, 0.4, or 0.6 mg/kg), 5A-APC (100 µg/kg), DFX (100 mg/kg), and/or GSHE (50 mg/kg), beginning at postnatal day 35. Disease onset was determined by rotarod analysis. All procedures were approved by the Institutional Animal Care and Use Committee at the University of Rochester and the University of Southern California. See *SI Materials and Methods* for details regarding rotarod analysis, definition of clinical death, tissue preparation, and blood sample collection for INR measurements. Mice were randomly assigned to treatment groups, and analyses were performed in a blinded fashion.

In Vitro Analyses. Primary neuronal cultures, primary mouse endothelial cells, and enriched motor-neuron cell preparations from *SOD1^{G93A}* mice were established as previously described. See *SI Materials and Methods* for details and references.

Brightfield Microscopy. Prussian blue staining and quantification of hemosiderin deposits were performed as described (9, 14).

Confocal Microscopy. Tissue sections were imaged with a custom-built Zeiss 510 Meta confocal laser scanning microscope with a Zeiss Aplanachromat 25×/0.8 NA water immersion objective (Carl Zeiss Microimaging). See *SI Materials and Methods* for details regarding immunofluorescent and fluorescent staining (Table S2), description of all antibodies used to detect endothelial cells (lectin and collagen IV), neurons (SMI-311, SMI-32, ChAT, and NeuN) and other antigens (e.g., 3-nitrotyrosine and ubiquitin), lasers and band-pass filters, regions analyzed, IgG accumulation, motor-neuron counts, neuritic density, ubiquitin accumulation, 3-nitrotyrosine, and quantifications methods.

Immunoblotting. Formation of detergent-soluble and insoluble SOD1 aggregation was analyzed as described (43). Tight junction proteins were analyzed as described (9). See *SI Materials and Methods* for details.

Biochemical Analyses. Free, chelatable iron levels and hemoglobin were quantified as described (44, 45). See *SI Materials and Methods* for details on protein carbonyl and sphingolipid measurements and RNA extraction and quantitative real-time PCR. For detailed description of primer sets, see Table S1.

Statistical Analysis. Log-rank tests with Bonferroni corrections for multiple comparisons were used to analyze treatment effect on symptom onset, survival, and lifespan. Correlations were determined using Pearson's correlation

analysis. Multifactorial analysis of variance, followed by Tukey post hoc tests, was used to compare treatment and genotype effects between groups. A *P* value < 0.05 was considered statistically significant for all studies.

ACKNOWLEDGMENTS. We thank J. Wang and S. Hillman for technical assistance with some experiments. This research was supported by ALS Association Grant 1859 and National Institutes of Health Grants AG039452, AG23084, and NS34467 (to B.V.Z.), HL031950 and HL052246 (to J.H.G.), and NS27036 (to D.W.C.). D.W.C. receives salary support from the Ludwig Institute for Cancer Research.

1. Zlokovic BV (2011) Neurovascular pathways to neurodegeneration in Alzheimer's disease and other disorders. *Nat Rev Neurosci* 12(12):723–738.
2. Kiernan MC, et al. (2011) Amyotrophic lateral sclerosis. *Lancet* 377(9769):942–955.
3. Winkler EA, et al. (2013) Blood-spinal cord barrier breakdown and pericyte reductions in amyotrophic lateral sclerosis. *Acta Neuropathol* 125(1):111–120.
4. Henkel JS, Beers DR, Wen S, Bowser R, Appel SH (2009) Decreased mRNA expression of tight junction proteins in lumbar spinal cords of patients with ALS. *Neurology* 72(18):1614–1616.
5. Miyazaki K, et al. (2011) Disruption of neurovascular unit prior to motor neuron degeneration in amyotrophic lateral sclerosis. *J Neurosci Res* 89(5):718–728.
6. Oba H, et al. (1993) Amyotrophic lateral sclerosis: T2 shortening in motor cortex at MR imaging. *Radiology* 189(3):843–846.
7. Kwan JY, et al. (2012) Iron accumulation in deep cortical layers accounts for MRI signal abnormalities in ALS: Correlating 7 tesla MRI and pathology. *PLoS ONE* 7(4):e35241.
8. Garbuzova-Davis S, et al. (2007) Evidence of compromised blood-spinal cord barrier in early and late symptomatic SOD1 mice modeling ALS. *PLoS ONE* 2(11):e1205.
9. Zhong Z, et al. (2008) ALS-causing SOD1 mutants generate vascular changes prior to motor neuron degeneration. *Nat Neurosci* 11(4):420–422.
10. Nicaise C, et al. (2009) Impaired blood-brain and blood-spinal cord barriers in mutant SOD1-linked ALS rat. *Brain Res* 1301:152–162.
11. Zhong Z, et al. (2009) Activated protein C therapy slows ALS-like disease in mice by transcriptionally inhibiting SOD1 in motor neurons and microglia cells. *J Clin Invest* 119(11):3437–3449.
12. Miyazaki K, et al. (2012) Early and progressive impairment of spinal blood flow-glucose metabolism coupling in motor neuron degeneration of ALS model mice. *J Cereb Blood Flow Metab* 32(3):456–467.
13. Armulik A, et al. (2010) Pericytes regulate the blood-brain barrier. *Nature* 468(7323):557–561.
14. Bell RD, et al. (2010) Pericytes control key neurovascular functions and neuronal phenotype in the adult brain and during brain aging. *Neuron* 68(3):409–427.
15. Bell RD, et al. (2012) Apolipoprotein E controls cerebrovascular integrity via cyclophilin A. *Nature* 485(7399):512–516.
16. Holbrook AM, et al. (2005) Systematic overview of warfarin and its drug and food interactions. *Arch Intern Med* 165(10):1095–1106.
17. Foerch C, et al. (2008) Experimental model of warfarin-associated intracerebral hemorrhage. *Stroke* 39(12):3397–3404.
18. Lauer A, et al. (2011) Anticoagulation with the oral direct thrombin inhibitor dabigatran does not enlarge hematoma volume in experimental intracerebral hemorrhage. *Circulation* 124(15):1654–1662.
19. Foerch C, You Z, Wang H, Lo EH, Whalen MJ (2012) Traumatic brain injury during warfarin anticoagulation: An experimental study in mice. *J Neurotrauma* 29(6):1150–1155.
20. Regan RF, Guo Y (1998) Toxic effect of hemoglobin on spinal cord neurons in culture. *J Neurotrauma* 15(8):645–653.
21. Boillée S, et al. (2006) Onset and progression in inherited ALS determined by motor neurons and microglia. *Science* 312(5778):1389–1392.
22. Beers DR, et al. (2006) Wild-type microglia extend survival in PU.1 knockout mice with familial amyotrophic lateral sclerosis. *Proc Natl Acad Sci USA* 103(43):16021–16026.
23. Di Giorgio FP, Carrasco MA, Siao MC, Maniatis T, Eggan K (2007) Non-cell autonomous effect of glia on motor neurons in an embryonic stem cell-based ALS model. *Nat Neurosci* 10(5):608–614.
24. Nagai M, et al. (2007) Astrocytes expressing ALS-linked mutated SOD1 release factors selectively toxic to motor neurons. *Nat Neurosci* 10(5):615–622.
25. Yamanaka K, et al. (2008) Astrocytes as determinants of disease progression in inherited amyotrophic lateral sclerosis. *Nat Neurosci* 11(3):251–253.
26. Haidet-Phillips AM, et al. (2011) Astrocytes from familial and sporadic ALS patients are toxic to motor neurons. *Nat Biotechnol* 29(9):824–828.
27. Gurney ME, et al. (1994) Motor neuron degeneration in mice that express a human Cu,Zn superoxide dismutase mutation. *Science* 264(5166):1772–1775.
28. Clement AM, et al. (2003) Wild-type nonneuronal cells extend survival of SOD1 mutant motor neurons in ALS mice. *Science* 302(5642):113–117.
29. Ferland G (2012) Vitamin K and the nervous system: An overview of its actions. *Adv Nutr* 3(2):204–212.
30. Ezzi SA, Urushitani M, Julien JP (2007) Wild-type superoxide dismutase acquires binding and toxic properties of ALS-linked mutant forms through oxidation. *J Neurochem* 102(1):170–178.
31. Gruzman A, et al. (2007) Common molecular signature in SOD1 for both sporadic and familial amyotrophic lateral sclerosis. *Proc Natl Acad Sci USA* 104(30):12524–12529.
32. Bosco DA, et al. (2010) Wild-type and mutant SOD1 share an aberrant conformation and a common pathogenic pathway in ALS. *Nat Neurosci* 13(11):1396–1403.
33. Polymenidou M, Cleveland DW (2011) The seeds of neurodegeneration: Prion-like spreading in ALS. *Cell* 147(3):498–508.
34. Pokrishevsky E, et al. (2012) Aberrant localization of FUS and TDP43 is associated with misfolding of SOD1 in amyotrophic lateral sclerosis. *PLoS ONE* 7(4):e35050.
35. Mosnier LO, Yang XV, Griffin JH (2007) Activated protein C mutant with minimal anticoagulant activity, normal cytoprotective activity, and preservation of thrombin activable fibrinolysis inhibitor-dependent cytoprotective functions. *J Biol Chem* 282(45):33022–33033.
36. Zlokovic BV, Griffin JH (2011) Cytoprotective protein C pathways and implications for stroke and neurological disorders. *Trends Neurosci* 34(4):198–209.
37. Mosnier LO, Zlokovic BV, Griffin JH (2007) The cytoprotective protein C pathway. *Blood* 109(8):3161–3172.
38. Jeong SY, et al. (2009) Dysregulation of iron homeostasis in the CNS contributes to disease progression in a mouse model of amyotrophic lateral sclerosis. *J Neurosci* 29(3):610–619.
39. Guizar-Sahagún G, et al. (2005) Glutathione monoethyl ester improves functional recovery, enhances neuron survival, and stabilizes spinal cord blood flow after spinal cord injury in rats. *Neuroscience* 130(3):639–649.
40. Vargas MR, Johnson DA, Johnson JA (2011) Decreased glutathione accelerates neurological deficit and mitochondrial pathology in familial ALS-linked hSOD1(G93A) mice model. *Neurobiol Dis* 43(3):543–551.
41. Ralph GS, et al. (2005) Silencing mutant SOD1 using RNAi protects against neurodegeneration and extends survival in an ALS model. *Nat Med* 11(4):429–433.
42. Chang HC, et al. (2008) Modeling spinal muscular atrophy in *Drosophila*. *PLoS ONE* 3(9):e3209.
43. Wang J, et al. (2003) Copper-binding-site-null SOD1 causes ALS in transgenic mice: Aggregates of non-native SOD1 delineate a common feature. *Hum Mol Genet* 12(21):2753–2764.
44. Nilsson UA, Bassen M, Sävman K, Kjellmer I (2002) A simple and rapid method for the determination of “free” iron in biological fluids. *Free Radic Res* 36(6):677–684.
45. Cheng T, et al. (2006) Activated protein C inhibits tissue plasminogen activator-induced brain hemorrhage. *Nat Med* 12(11):1278–1285.